https://doi.org/10.5194/egusphere-2022-48
Preprint. Discussion started: 27 April 2022

Extreme wet-cold compound events investigation under climate change in Greece

Iason Markantonis[1,2], Diamando Vlachogiannis[1], Athanasios Sfetsos[1], Ioannis Kioutsioukis[2]

[1]Environmental Research Laboratory, NCSR "Demokritos", 15341 Agia Paraskevi, Greece
[2]University of Patras, Department of Physics, University Campus 26504 Rio, Patras, Greece

Correspondence to: Iason Markantonis (jasonm@ipta.demokritos.gr)

Abstract. This paper aims to study wet-cold compound events (WCCEs) over Greece for the wet and cold season November-April. WCCEs are divided in two different compound events (TX-RR) and (TN-RR) and two different approaches using fixed (RR over 20 mm/day and Temperature under 0 °C) and percentile (RR over 95th and Temperature under 5th) thresholds. Observational data from the Hellenic National Meteorology Service (HNMS) and simulation data from reanalysis and EUROCORDEX models were used in the study for the historical period 1980-2004. Simulation datasets from projection models were employed for the near future period (2025-2049) to study the impact of climate change on the occurrence of WCCEs under RCP 4.5 and 8.5 scenarios. Following data processing and validation of the models, the potential changes in the distribution of WCCEs in the future were investigated based on the projected and historical simulations. WCCEs determined by fixed thresholds were mostly found over high altitudes with a future tendency to reduce particularly under RCP 8.5. On the other hand, WCCEs obtained with percentile thresholds, were distributed mostly in Eastern Greece and Crete while their changes differed significantly among models.

1. Introduction

Extreme weather events and their linkage to climate change is a matter of high concern for many scientific groups (Zanocco et al., 2018; Konisky et al., 2016; Curtis et al., 2017). In the last decade numerous scientific researches focused on the causes, the frequency and impacts of extreme compound events (e.g. Aghakouchak et al., 2020; Singh et al., 2021; Sadegh et al., 2018; Zscheischler et al., 2017; Zscheischler and Seneviratne, 2017; Zscheischler et al., 2018). As mentioned in IPCC SREX (Ref 7, p. 118) compound events are defined as: (1) two or more extreme events occurring simultaneously or successively, (2) combinations of extreme events with underlying conditions that amplify the impact of the events, or (3) combination of events that are not themselves extremes but lead to an extreme event or impact when combined. The contributing events can be of similar (clustered multiple events) or different type(s) (Leonard et al., 2014).

The purpose of this article is the study of extreme wet-cold compound events (WCCEs) in Greece during the historical period (1980-2004) and how the occurrence of these events will be affected by climate change. using projection data from and . It has been reported that WCCEs affect the region of Mediterranean Sea, including Greece (Zhang et al., 2021). The examined events belong to the first category of the definition of compound events from IPCC since they refer to the simultaneous exceedance of precipitation and temperature thresholds. WCCEs can have negative impact on people's lives by causing electricity blackouts, affecting agriculture with heavy snowfall or freezing rain, blocking transportation because of closed roads, railways or even airports (Houston et al., 2006; Llasat et al., 2014; Vajda et al., 2014). On the other hand, most of the available freshwater in the country comes from melted mountain snow during spring or summer. Finally, eco-systems, especially on mountains, may be harmed by the absence of snow that climate change may cause (Demiroglu et al., 2015; Pestereva et al., 2012; Trujillo et al., 2012; García-Ruiz et al., 2011). Moreover, Athens, a city of more than 4 million inhabitants, experienced in two consecutive years snowstorms (16, 17 February 2021 and 24 January 2022), which caused great problems in road traffic and electricity failures.. Historically, such events occur infrequently in the region and it is the first time that snow depth exceeds 15cm twice in a period of

https://doi.org/10.5194/egusphere-2022-48
Preprint. Discussion started: 27 April 2022

eleven months in the city center At other parts of Greece such events are more frequent, and this is shown in the present study.

This work extends further and more meticulously the study of Markantonis et al., (2021) about daily minimum temperature and accumulated precipitation WCCEs. The motivation is the absence of such similar study concerning the country, with few exceptions that used only observational data at some locations (Lazoglou and Anagnostopoulou, 2019), or modeled data mostly over the broader region of Mediterranean Sea lacking detailed analysis for Greece (Vogel et al., 2021; Hochman et al., 2021; de Luca et al., 2020). The greatest part of the study concerns the historical period between 1980 and 2004, because of the availability of quality controlled daily observational data for minimum temperature (TN), maximum temperature (TX) and accumulated precipitation (RR). Thence, for that period, we use observational data from 21 Hellenic National Meteorological Service (HNMS) stations, for the validation of EURO-CORDEX Regional Climate Models (RCMs), provided by the Climate Change Service of EUs Copernicus Program and the projection model dataset produced in-house. In addition to the models, two reanalysis products are included, as the closest to true past climate conditions in regions with no or scarce observations (Moalafhi et al., 2016). More information about the observational and model datasets is shown in Section 2. Section 3 highlights the applied methodology while Section 4 presents the comparison of model data with observations. Section 5, details the results about the WCCEs for the historical period and the projected changes by each model for the near future period between 2025 and 2049 for two greenhouse gas concentration scenarios, RCP 4.5 and RCP 8.5.

2. Data

2.1 HNMS observations

HNMS provides freely observational data from 21 stations for the purpose of scientific research. The data have been formally evaluated by HNMS and the timeseries show no missing or distorted values. In particular, the timeseries available for the historical period 1980-2004 have a 3-hour temporal resolution and from these values we have extracted the daily values of TN, TX and RR. Figure 1 shows the position of the stations while Table A1 of Appendix A provides details on the characteristics of the stations . We have used the observational data to validate the model datasets with regard to the WCCEs for the historical period.

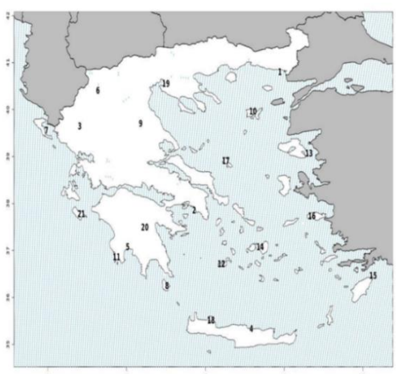

Figure 1: Map of HNMS stations. The numbers correspond to those in Table A1 (Appendix A).

2.2 Reanalysis models

https://doi.org/10.5194/egusphere-2022-48
Preprint. Discussion started: 27 April 2022

We have used two reanalysis models due to the lack of spatially and temporally complete direct observations, to study more consistently the WCCEs in Greece in the historical period. The first model is the latest available reanalysis product ERA 5 from ECMWF of spatial resolution ~30km x 30km (Hersbach et al., 2020). The second reanalysis model, built in Environmental REsearch Laboratory (EREL) of National Center of Scientific Research 'Demokritos' (NCSRD) WRF_ERA_I, has been produced by dynamically downscaling ERA-INTERIM using the Weather Research Forecast (WRF) model (v3.6.1) from 80km x 80km to 5km x 5km (Politi et al., 2021, 2020, 2018).

2.3 GCM / RCM models

To observe possible alterations of wet-cold compound events occurrence probability in the future period 2025-2049 compared to the historical period, we employed data from RCM simulations driven by GCMs. In this regard, we obtained data from 5 models included in the EURO-CORDEX initiative provided by the Copernicus Program. All chosen models have a spatial resolution of 0.11° x 0.11° and available daily data for both RCP scenarios. Information on the regional and parent models and their acronyms used herewith is given in Table 1. In addition to the EURO-CORDEX model data, we have used dynamically downscaled data from the EC-EARTH GCM to high spatial resolution of 5km x 5km for the area of Greece using WRF (Politi et al., 2020, 2022)

Institution	Reference	Regional Model	Forcing model	Acronym	Resolution (°)
Météo-France / Centre National de Recherches Météorologiques	(Spiridonov et al., n.d.)	ALADIN63	CNRM-CERFACS-CNRM-CM5	CNRM	0.11
Koninklijk Nederlands Meteorologisch Instituut	(van Meijgaard et al., 2008)	KNMI-RACMO22E	ICHEC-EC-EARTH	KNMI	0.11
Climate Limited-Area Modelling Community	(Rockel et al., 2008)	CLMcom-CLM-CCLM4-8-17	MOHC-HadGEM2-ES	CLMcom	0.11
Swedish Meteorological and Hydrological Institute	(Samuelsson et al., 2016)	SMHI-RCA4	MPI-M-MPI-ESM-LR	SMHI	0.11
Danish Meteorological Institute	(Christensen, 2006)	DMI-HIRHAM5	NCC-NorESM1-M	DMI	0.11
EREL (NCSRD)	(Politi et al. 2020, 2022)	ARW-WRF	EC-EARTH	WRF_EC	0.05

Table 1: EURO-CORDEX and EREL-NCSRD simulation models information.

3 Methodology

The process we followed in this work is briefly presented in the flowchart of Figure 2. The light blue steps form the main flow of the approach that mainly include the selection of the compound events based on threshold criteria, validation of the obtained compounds against observational data, and calculation of their occurrence probabilities. The models' validation part is a previous step to the exhibition of

https://doi.org/10.5194/egusphere-2022-48
Preprint. Discussion started: 27 April 2022

modeled data and is added on the data processing step. At the validation step we also compare univariate 20-year return levels using two different approaches, Peaks Over Threshold (POT) and Block Maxima or Minima (BM), further described in section 4.2.2. The calculated probabilities of WCCEs using all models in the historical period have been validated against observations. The yellow boxes describe the results displayed at each step.

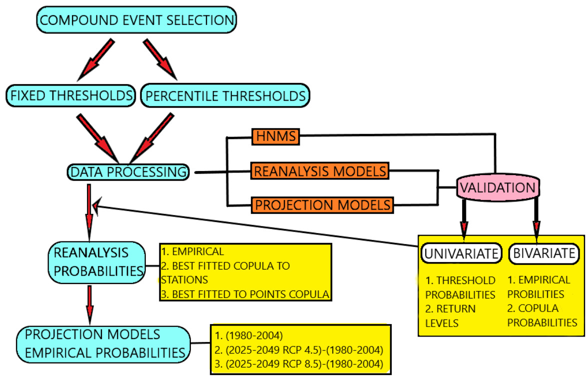

Figure 2: WCCEs methodology process flowchart.

In the later sections, we use box-plots to depict the ability of the models to simulate observational data for the historical period at the cells that include meteorological stations. The box-plots consist of the colored box, where in the band near the middle of the box is the median, the bottom and top of each color box are the 25th and 75th percentile (BL) and the ends of the whiskers are the 1.5 times the difference between the 25th and 75th percentiles (WL).

3.1 Compound event selection

According to HNMS the meteorological year can be split into two climate periods (http://emy.gr/emy/el/climatology/climatology). The cold and wet period extends on average from mid-October to the end of March, and the warm-dry period occurs during the rest of the year. Since the study is focused on the extreme WCCEs, we examine the period between November and April, since according to HNMS observations, April exhibits lower temperatures than October and more rainy days. Moreover, it is not uncommon for the northern parts of Greece, and especially mountainous areas, to be affected by snowfalls during April. This leads to the creation of a timeseries of 4532 daily values for the historical period and 4531 for the future period. The only exception is CLMcom which considers that each month is consisted by 30 days, thus leading to 4500 values for each period. The near-neighbour approach revealed the nearest to the station grid cell.

The WCCEs, which are examined on daily basis, are divided in two types of synchronous events, TX-RR and TN-RR and studied using two different approaches, (1) the percentile threshold and (2) the fixed threshold (Table 2). For the first method the thresholds are the 95th percentile of RR distribution and the 5th percentile of TN and TX distribution. This approach examines the threshold for each variable at each station or grid point. The second approach considers the fixed threshold of 20 mm/day for RR and 0 °C for TN and TX for all stations or grid points. TN equal to or under 0 °C indicates Frost Days (FD), while TX equal or under 0 °C Iced Days (ID) (Fonseca et al., 2016). Firstly, we compare the univariate exceedance probabilities and then the bivariate ones. The difference between the two methods is that the percentile approach calculates the probability that an event considered extreme for the study area occurs, while the second that an event considered already extreme occurs. The thresholds examined have been proposed in various studies for both univariate and bivariate cases (Raziei et al., 2014; Tošić and Unkašević, 2013; Anagnostopoulou and Tolika, 2012; Pongrácz et al., 2009; Kundzewicz et al., 2006; Moberg et al., 2006)

THRESHOLDS	RR	TN	TX	WCCE

FIXED	>= 20 mm/day **(RR20)**	<= 0 ºC **(FD)**	<= 0 ºC **(ID)**	1. **(RR20-FD)** 2. **(RR20-ID)**
PERCENTILE	>= 95th **(RR95p)**	<= 5th **(TN5p)**	<= 5th **(TX5p)**	1. **(RR95p-TN5p)** 2. **(RR95p-TX5p)**

Table 2: Univariate thresholds and the compound events examined in the study.

3.2 WCCEs probability calculation

The WCCEs probabilities are calculated applying two different methods. The first is the empirical approach counting the events from the timeseries and dividing by the total number of days to find the percentage (%) of the occurrence probability. For the second method, we use the copula approach for the HNMS observations and models comparison and to map the differences of the two methods for the reanalysis model data. Compared to copula, an empirical method has a higher uncertainty when calculating the probability of extreme events (Hao et al., 2018; Tavakol et al., 2020; Zscheischler and Seneviratne, 2017). The purpose of using two different methods is to examine whether the copula method underestimates or overestimates the WCCEs.

The best fitting copula selection for each timeseries is done using the R programming language function BiCopSelect, included in the package VineCopula (Schepsmeier et al., 2013). The appropriate bivariate copula for each dataset is chosen, by the function, from a multitude of 40 different copula families using the Akaike Information Criterion (AIC) (Akaike, 1974), and the copula chosen for each station and model dataset is shown in Appendix B (Tables B1 and B2). Copulas are used in plenty of studies that investigate the dependence between two different climate variables and the joint probability of compound events (Tavakol et al., 2020; Dzupire et al., 2020; Pandey et al., 2018; Cong and Brady, 2012; Abraj and Hewaarachchi, 2021).

As mentioned in Nelsen, (2007), a bivariate copula is a bivariate distribution function where margins are uniform on the unit interval [0, 1]. A bivariate copula is a map $C:[0,1]^2 \rightarrow [0,1]$ with $C(u,1)=u$ and $C(1,v)=v$. Let X and Y be random variables with a joint distribution function $F(x,y)=Pr(X \le x, Y \le y)$ and continuous marginal distribution functions $F_1(x)=Pr(X \le x)$ and $F_2(y)=Pr(Y \le y)$, respectively. By Sklar's theorem (Sklar, 1959), one obtains a unique representation

$$F(x,y) = C\{F_1(x),F_2(y)\} \quad (1)$$

For the two random variables of X (e.g., precipitation) and Y (e.g., temperature) with cumulative distribution functions (CDFs) $F_1(x)=Pr(X>=x)$ and $F_2(y)=Pr(Y<=y)$, the bivariate joint distribution function or copula (C) can be written as:

$$F(x,y) = Pr(X>=x,Y<=y) = C(u,v) \quad (2)$$

Besides copula probabilities, we also show the Kendall rank correlation and tail dependence (χ) between the variables (RR–TN) and (RR-TX) to examine the dependence between the variables over all the range and tails of the distribution.

The Kendall rank correlation coefficient evaluates the degree of similarity between two sets of ranks given to a same set of objects (Abdi, 2007) and we prefer it from other correlation types because it provides a distribution free test of independence and a measure of the strength of dependence between two variables. Kendall's tau (τ) is given by Eq. 3, and has a range [-1, 1]:

$$\tau = (Nc–Nd) /(n*(n-1) / 2 \quad (3)$$

where, Nc is the number of concordant pairs and Nd the number of discordant pairs.

Tail dependence describes the limiting proportion that one margin exceeds a certain threshold given that the other margin has already exceeded that threshold that has a range [0, 1]. In R, we use the function taildep from package extRemes (Gilleland and Katz, 2016) for the threshold u=0.95 to calculate Chi (χ). Chi is calculated by:

https://doi.org/10.5194/egusphere-2022-48
Preprint. Discussion started: 27 April 2022

$$chi(u) = Pr[Y > G^{-1}(u) \mid X > F^{-1}(u)] = Pr[V > u \mid U > u], \quad (4)$$

where (U, V) = (F(X), G(Y))--i.e., the copula.

4 Results in observation locations

In this section, we firstly examine the dependence between the variables based on the HNMS data and using these data we calculate the probability of WCCEs applying both empirical and copula approaches. Then, we use the HNMS data to validate both reanalysis and projection models during the historical period.

4.3 HNMS WCCE climatology

Figure 3 presents the tail dependence for the two different types of compound events examined. Only two stations in Crete show minor dependence between the variables at the tails of the distributions. Figure 4 shows that (RR20-FD) events are located mostly in the mainland, while RR95p-TN5p in the Aegean Sea area. At several stations, there is a difference between the empirical and the copula approach, which usually overestimates the total number of WCCEs. In Figure 5a only two stations show a significant number of RR20-ID events. At the percentile threshold approach (Figure 5b), we observe few WCCEs using the empirical method, while all stations show a significant number of WCCEs using the copula method.

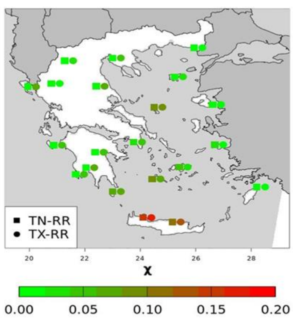

Figure 3: Tail dependence (χ) for TN-RR (squares) and TX-RR (circles).

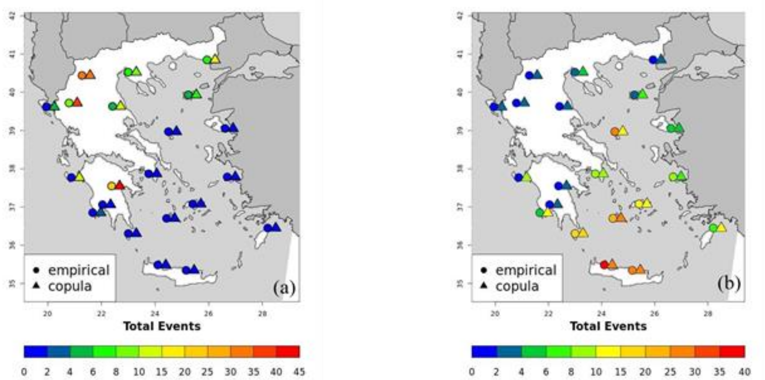

Figure 4: Total number of WCCEs (1980-2004) for (a) RR20-FD and (b) RR95p-TN5p.

https://doi.org/10.5194/egusphere-2022-48
Preprint. Discussion started: 27 April 2022

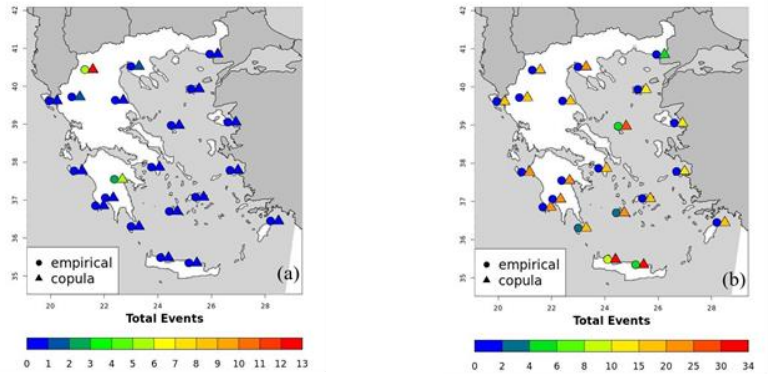

Figure 5: Total number of WCCEs (1980-2004) for (a) RR20-ID and (b)RR95p-TX5p.

4.4 Univariate validation

Both reanalysis and projections models are compared to observational data for each variable and for the WCCEs probabilities. Figures 6-8 present the mean values and the standard deviation for stations and the respective models' grid points. The corresponding values for each station are shown in Tables S1-S3 and S5-S7 from Supplementary material.

4.2.1 Thresholds & Probabilities

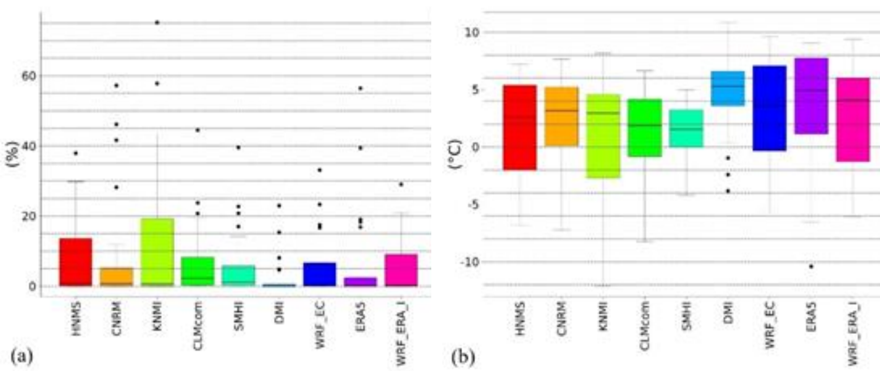

Figure 6: Boxplots of (a) FD probability and (b)TN5p threshold.

https://doi.org/10.5194/egusphere-2022-48
Preprint. Discussion started: 27 April 2022

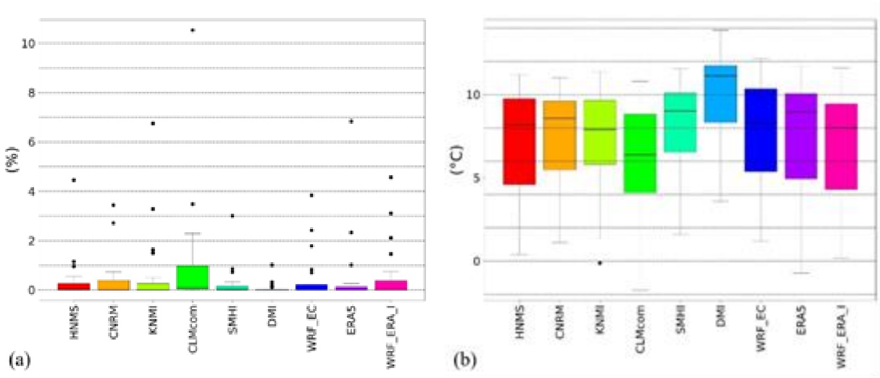

Figure 7: Boxplots of (a) ID probability and (b)TX5p threshold.

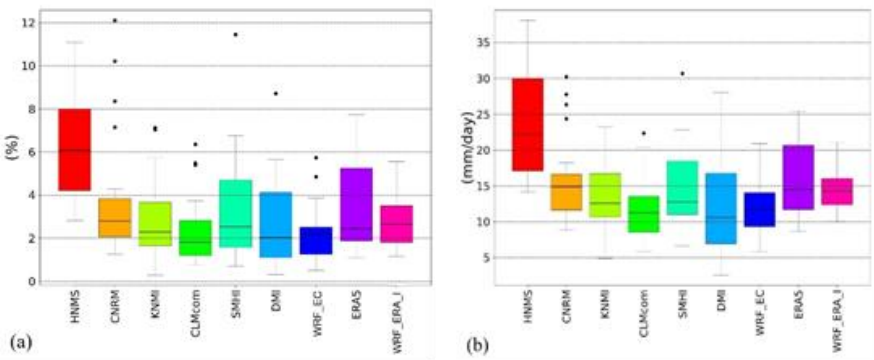

Figure 8: Boxplots of (a) RR20 probability and (b)RR95p threshold.

For TN and TX (Figures 6 and 7, respectively) seems to be a good concordance of most models mean values with the HNMS data, although there are differences in the range of BL and WL between the models. The model that mostly overestimates TX5p and TN5p thresholds is DMI. For RR (Figure 8), all models underestimate extreme values compared to HNMS with ERA5 being closer to observations.

4.2.2 Return levels

Another way to compare extreme values is the calculation of return levels. As mentioned in methodology we use two approaches, (BM) and (POT). For BM we use the annual maximum or minimum value of the variable that results in the loss of information, because there is available only one value per year. BM samples tend to follow the GEV distribution, according to The Fisher–Tippett–Gnedenko theorem (Fisher and Tippett, 1928; Gnedenko, 1943). For BM we fit the GEV by applying the method 'Lmoments' using the function fevd from R package extRemes.

On the other hand, POT has the advantage of examining more values per year with the chosen condition that the values above the right threshold are considered as extreme (Balkema and Haan, 1974; James Pickands, 1975). The approach is to select as threshold the 90th percentile of the variable distribution (Bommier, 2014). Also, in order to achieve that each extreme value is independent from another, we use a conservative 5-day threshold declustering (Coles, 2001), securing that there are no extreme values affected by the same synoptic system. For POT we fit the Generalized Pareto (GP) distribution, which corresponds to the tail distribution of the GEV (Goda, 2018). As suggested in Poschlod, (2021), we use

https://doi.org/10.5194/egusphere-2022-48
Preprint. Discussion started: 27 April 2022

Maximum Likelihood Estimation (MLE) as an optimization algorithm to fit the GP to the declustered timeseries, using again the extRemes package.

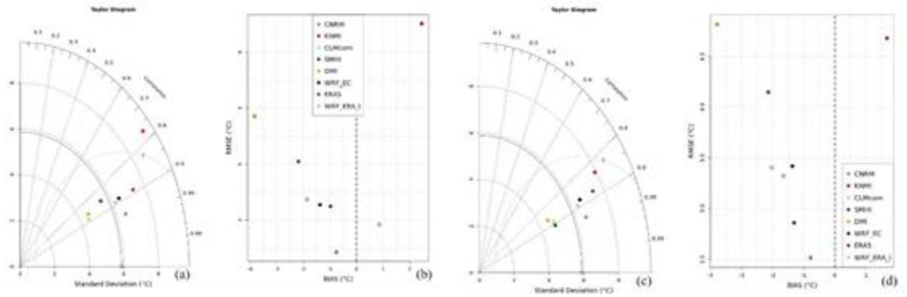

Figure 9: Taylor diagram for TN 20 years return level using (a) POT and (c) BM approach. RMSE-BIAS plots for (b) POT and (d) BM.

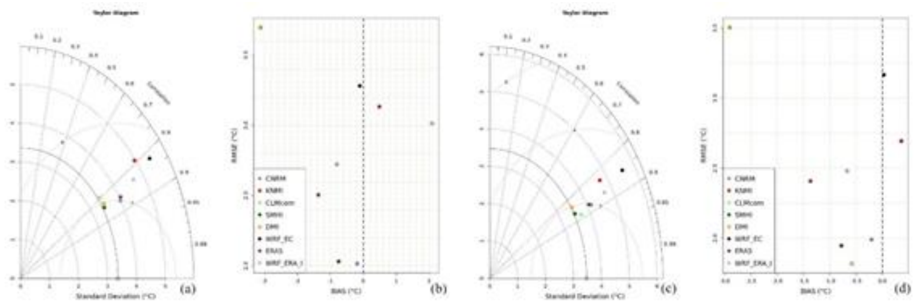

Figure 10: Taylor diagram for TX 20 years return level using (a) POT and (c) BM approach. RMSE-BIAS plots for (b) POT and (d) BM.

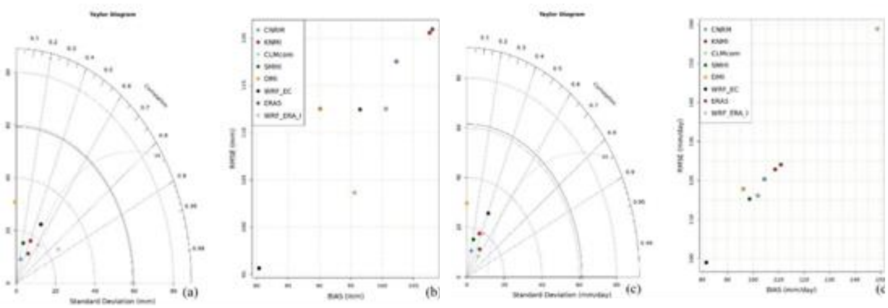

Figure 11: Taylor diagram for RR 20 years return level using (a) POT and (c) BM approach. RMSE-BIAS plots for (b) POT and (d) BM.

Figures 9 and 10 show that the CNRM is the model closer to HNMS TN and TX 20 years return level. Figure 11 yields that WRF_ERA_I has the highest correlation to observations, while WRF_EC the best RMSE-BIAS relation to observations. The values used to produce Figures 9-11 can be found in Tables S11-S16 from Supplementary material.

4.5 Bivariate validation

https://doi.org/10.5194/egusphere-2022-48
Preprint. Discussion started: 27 April 2022

The bivariate validation of the models is conducted by the empirical and copula methods for the WCCEs at the stations. Figures 12 and 13 summarize the results from Supplementary material Tables S4, S5 and S9, S10, respectively.

4.5.1 Empirical approach

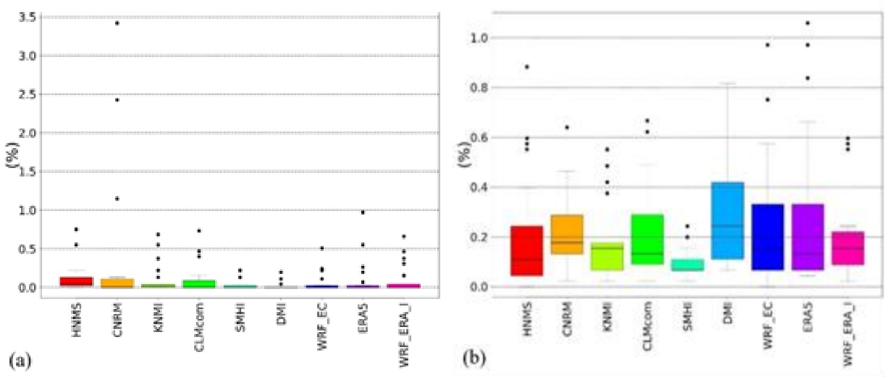

Figure 12: Boxplots of probabilities for (a) RR20-FD and (b) RR95p-TN5p WCCEs.

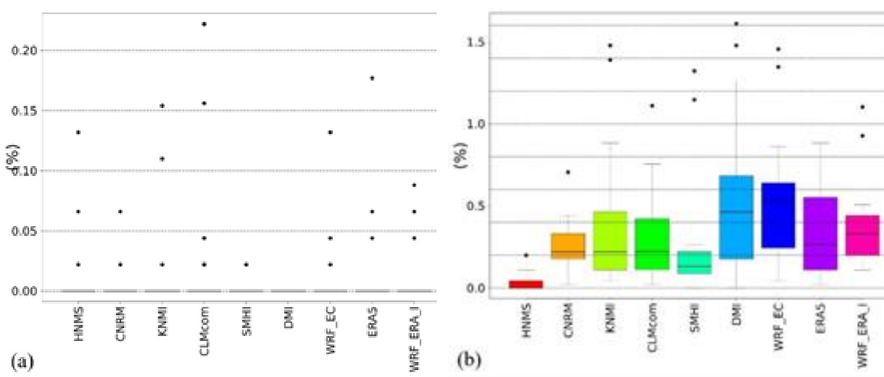

Figure 13: Boxplots of probabilities for (a) RR20-ID and (b) RR95p-TX5p WCCEs.

In Figure 12a, HNMS BL is greater than all models, although a number of models show values greater than the WL of observations, with CNRM yielding the most extreme values, with 3 cases of more than 1% probability. RR95p-TN5p events probabilities from models are close or over the mean values and BL of HNMS except for the case of SMHI which shows smaller values (Figure 12b). From Figure 13a we find that RR20-ID events are extremely rare at the locations of the stations with few exceptions. DMI exhibits zero events, while the largest probabilities are exhibited by CLMcom with four non-zero probabilities points . In Figure 13b, we see that all models overestimate the probabilities of RR95p-TX5p events with DMI showing the highest probabilities and SMHI the closer to HNMS agreement.

https://doi.org/10.5194/egusphere-2022-48
Preprint. Discussion started: 27 April 2022

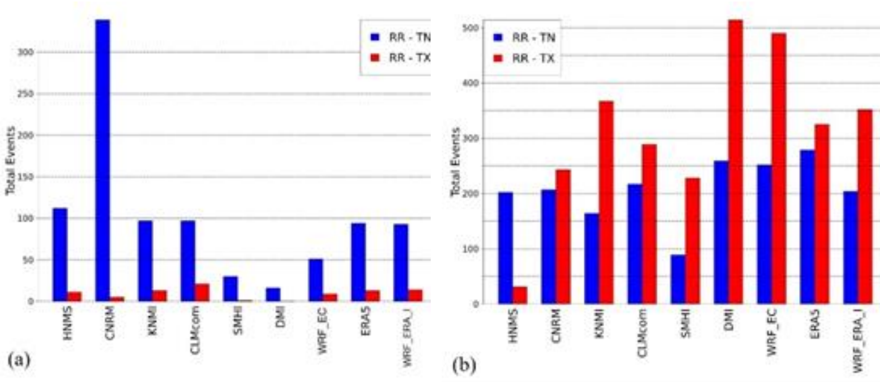

Figure 14: Bar-plots of total number of WCCEs for (a) fixed and (b) percentile thresholds for the 1980-2004 period.

In Figure 14, we present a quantitative comparison of the total number of compound events that are counted for all stations and the corresponding grid points for each model. For fixed thresholds, most models show good agreement with the HNMS data except of CNRM which overestimates the amount of total WCCEs for the RR-TN case. Also, SMHI and DMI and to a lesser extent WRF_EC underestimate significantly the number of total events for both types. With the percentile threshold approach all models overestimate the number of WCCEs for the RR-TX case, while for the RR-TN case most models are close to the HNMS total number of WCCEs, except of SMHI which underestimates it.

4.5.2 Copula approach

The best-fitted copulas fixed and percentiles probabilities for each model dataset are compared to the respective HNMS station best-fitted copula in Figures 15 and 16, respectively. We use Taylor diagrams and RMSE-BIAS plots to observe which models are closer to the WCCEs probabilities calculated for the HNMS data.

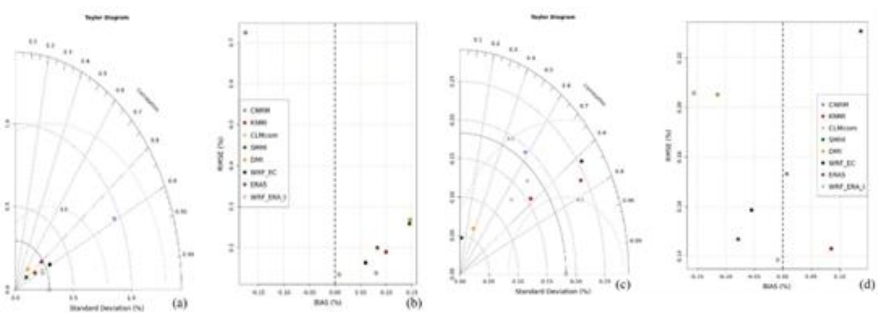

Figure 15: Taylor diagram of WCCEs copula probabilities for (a) RR20-FD and (c) RR95p-TN5p. RMSE-BIAS plots of WCCEs copula probabilities for (b) RR20-FD and (d) RR95p-TN5p.

https://doi.org/10.5194/egusphere-2022-48
Preprint. Discussion started: 27 April 2022

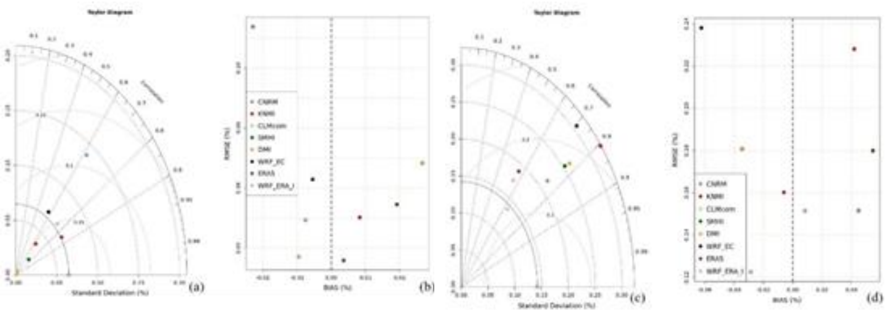

Figure 16: Taylor diagram of WCCEs copula probabilities for (a) RR20-ID and (c) RR95p-TX5p. RMSE-BIAS plots of WCCEs copula probabilities for (b) RR20-ID and (d) RR95p-TX5p.

Figures 15 and 16 show that models agree more with observations on fixed thresholds WCCEs than the percentiles ones, where there is a broader deviation of correlation to observations. Probabilities for WCCEs are generally close to zero for observations and models, therefore RMSE and BIAS values are also almost zero. The values for each station are presented analytically in Tables S19-S22 from the Supplementary material.

5 Models

5.1 Reanalysis

Data from reanalysis models provide us with information on the WCCEs for the historical period, at places with no available observational data. Thus, we will examine the probability of WCCEs using three different methods for the reanalysis data. (1) The empirical probability method, (2) the probability calculated by the most common copula from the total of the 21 HNMS stations and (3) the best-fitted copula at each grid point of the model. For comparison, we show the differences between each pair of methods. The reason to show the second method is to examine its ability to resemble the empirical method, since it is computationally much faster than method (3). In Tables B1 and B2 of Appendix B it is shown that the best fitted copula for HNMS timeseries is the Rotated BB8 270 degrees for (-TN, RR) bivariate distribution and the Survival BB8 for (-TX, RR) bivariate distribution. In both cases, the copulas are chosen for 10 out of the 21 stations. In the appendix, the univariate probabilities and thresholds are also shown. Firstly, we show the Kendall rank correlation (τ) (Figure 17) and then the tail dependence (χ) (Figure 18) between the variables. For the sake of brevity, we refer to the three methods as (A), (B) and (C).

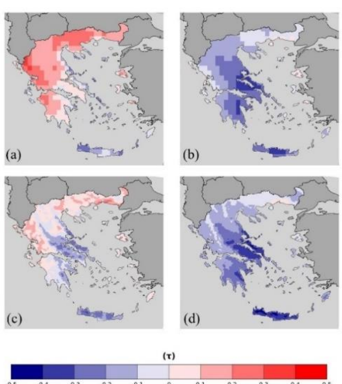

https://doi.org/10.5194/egusphere-2022-48
Preprint. Discussion started: 27 April 2022

Figure 17: Kendall rank correlation (τ) between (a, c) TN-RR and (b, d) TX-RR and (a, b) ERA 5 and (c, d) WRF_ERA_I.

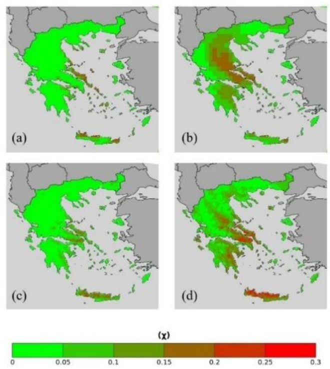

Figure 18: Tail dependence (χ) at 95% between (a, c) TN-RR and (b, d) TX-RR and (a, b) ERA 5 and (c, d) WRF_ERA_I.

Figure 17 shows that there is little correlation between the variables with TN-RR having mostly slight positive correlation (17a, 17c), while more negative correlation reaching to -0.5 is calculated for TX-RR (17b, 17d). From tail dependence for the 5 % of the distributions in Figure 18, we see that TX-RR (18a, 18c) are more dependent from TN-RR (18b, 18d) in more regions of the map. Values reach up to 0.3 mainly for TX-RR in eastern Greece and Crete. Also, Figures S1-S3 in th supplementary material present the univariate thresholds and probabilities for RR, TN and TX using the reanalysis datasets (ERA5 and WRF_ERA_I).

5.1.1 TN-RR WCCEs

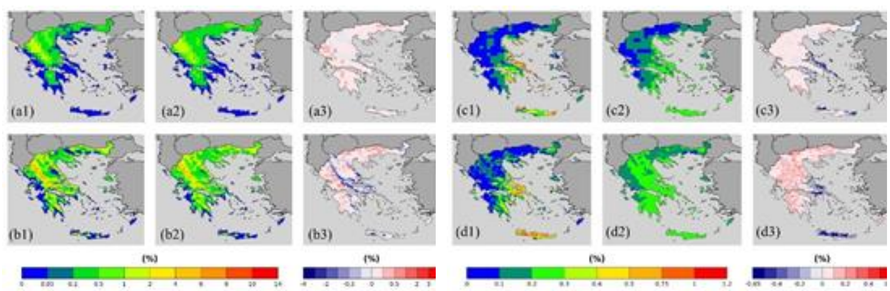

Figure 19: (a, b) RR20-FD and (c, d) RR95p-TN5p WCCEs probabilities. (a, c) ERA 5 and (b, d) WRF_ERA_I. Column (1) is method A, (2) method B and (3) = (2) – (1).

https://doi.org/10.5194/egusphere-2022-48
Preprint. Discussion started: 27 April 2022

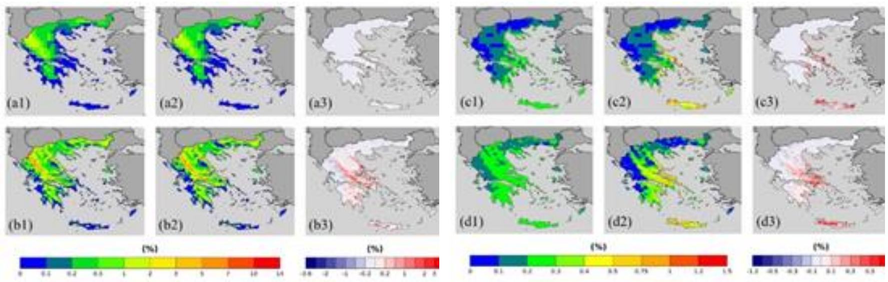

Figure 20: (a, b) RR20-FD and (c, d) RR95p-TN5p WCCEs probabilities. (a, c) ERA 5 and (b, d) WRF_ERA_I. Column (1) is method B, (2) method C and (3) = (2) – (1).

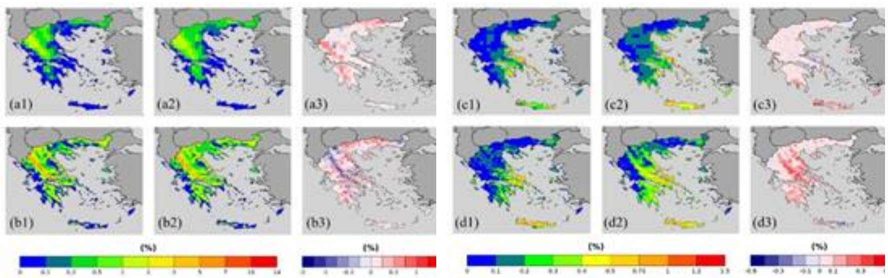

Figure 21: (a, b) RR20-FD and (c, d) RR95p-TN5p WCCEs probabilities. (a, c) ERA 5 and (b, d) WRF_ERA_I. Column (1) is method A, (2) method C and (3) = (2) – (1).

From Figures 19 and 20 we observe that method B underestimates the extreme value probabilities compared to methods A and C. On the other hand, method B exhibits less non-zero values compared to method A. In Figure 21, we see that method C mostly overestimates WCCEs compared to method A, especially for RR95p-TN5p and WRF_ERA_I. RR20-FD events reach at most extreme probabilities of 14%, while for RR95p-TN5p the highest probabilities range between 1.2% and 1.5%.

5.1.2 TX-RR WCCEs

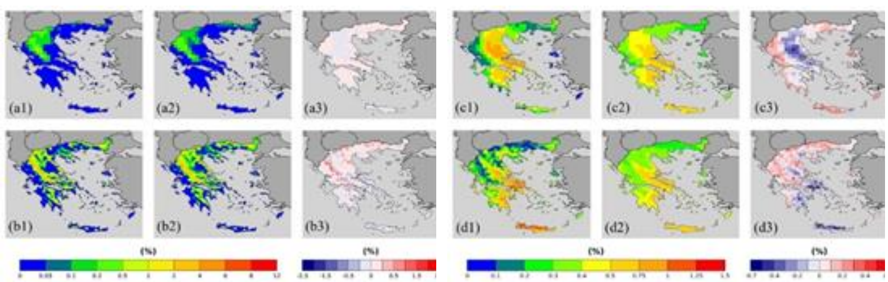

Figure 22: (a, b) RR20-ID and (c, d) RR95p-TX5p WCCEs probabilities. (a, c) ERA 5 and (b, d) WRF_ERA_I. Column (1) is method A, (2) method B and (3) = (2) – (1).

https://doi.org/10.5194/egusphere-2022-48
Preprint. Discussion started: 27 April 2022

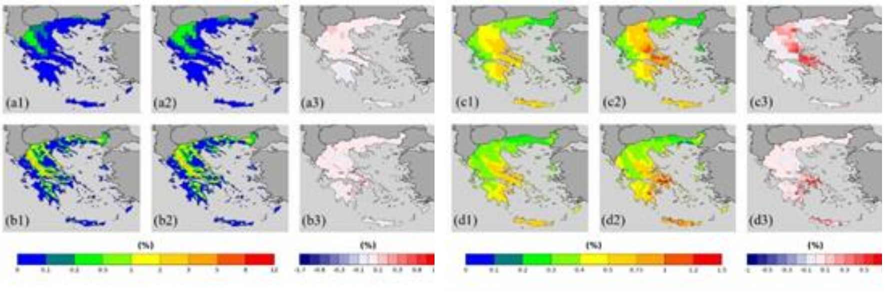

Figure 23: (a, b) RR20-ID and (c, d) RR95p-TX5p WCCEs probabilities. (a, c) ERA 5 and (b, d) WRF_ERA_I. Column (1) is method B, (2) method C and (3) = (2) – (1).

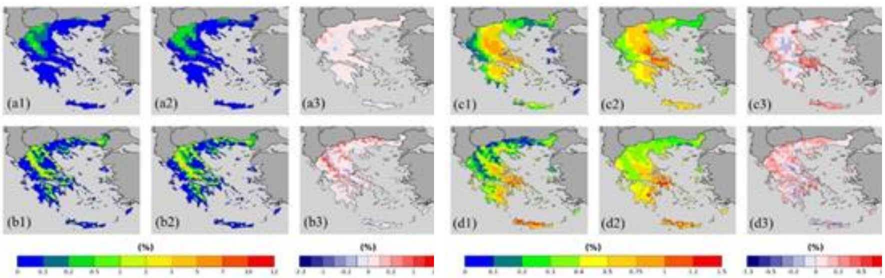

Figure 24: (a, b) RR20-ID and (c, d) RR95p-TX5p WCCEs probabilities. (a, c) ERA 5 and (b, d) WRF_ERA_I. Column (1) is method A, (2) method C and (3) = (2) – (1).

Figures 22-24 show that RR20-ID events exhibit lower probabilities than RR20-FD events reaching 10% to 12%. RR95p-TX5p reach 1.5% at the most extreme values, which are distributed at a greater area than RR95p-TN5p. On the other hand, method C exhibits the highest probabilities for both approaches events.

5.2 Past-Future Projections comparison

The six projection models we previously evaluated, are used here to study their behavior in the calculation of the probabilities of WCCEs. We compare the historical period probabilities with the probabilities determined for the future scenarios RCP 4.5 and RCP 8.5 for the 2025-2049 period by applying both fixed thresholds and percentiles. The differences mapped are statistically significant at 95% level using the Student's t-test (Goulden, 1939) comparing 25 annual values of the timeseries. We have applied the empirical method to calculate the probabilities of the WCCEs. Univariate thresholds and probabilities are shown in Figures S4-S6 of the supplementary material.

https://doi.org/10.5194/egusphere-2022-48
Preprint. Discussion started: 27 April 2022

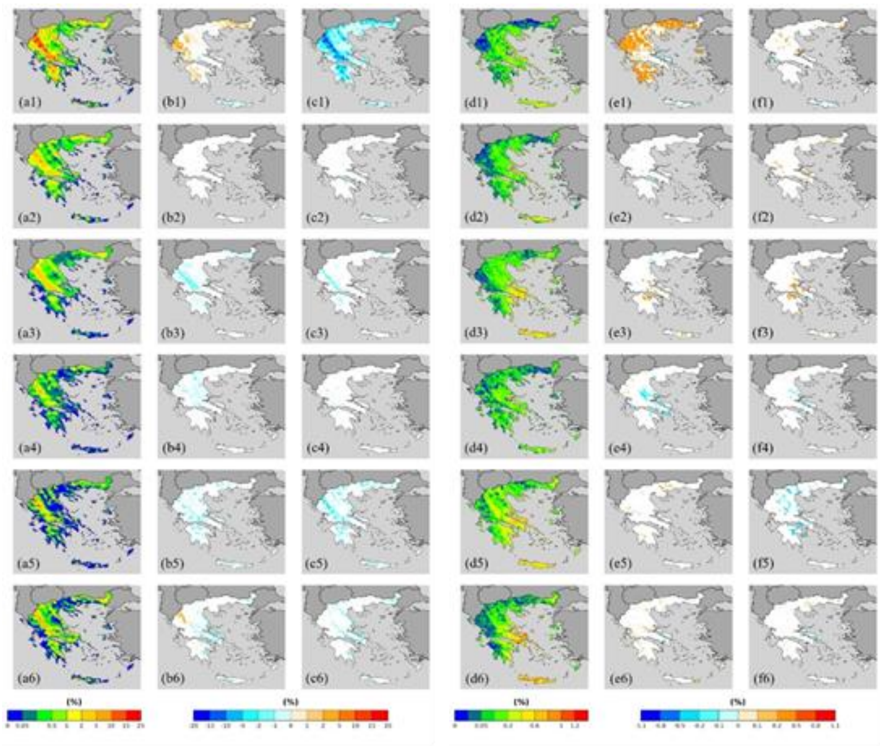

Figure 25: (a-c) RR20-FD and (d-f) RR95p-TN5p probabilities. Models 1: CNRM, 2: KNMI, 3: CLMcom, 4: SMHI, 5: DMI, 6: WRF_EC. (a, d) 1980-2004, (b, e) (2025-2049 RCP 4.5) – (1980-2004) and (c, f) (2025-2049 RCP 8.5) – (1980-2004).

We see from Figure 25a that RR20-FD events probabilities may reach 25% particularly for CNRM, which also exhibits the greatest changes in the future, being mostly positive for RCP4.5 and extremely negative (up to -20%) for RCP8.5. Other models calculate fewer extreme probabilities for RR20-FD events and less extreme changes in the future being mostly negative and found in mountainous areas. RR95P-TN5p events displayed in Figure 25d reach up to 1.5% only for WRF_EC. The rest of the models reach most extreme values in the range of 0.4% to 1%. Most models do not display significant changes in the future, except of CNRM which shows positive changes that spread extensively over Greece.

https://doi.org/10.5194/egusphere-2022-48
Preprint. Discussion started: 27 April 2022

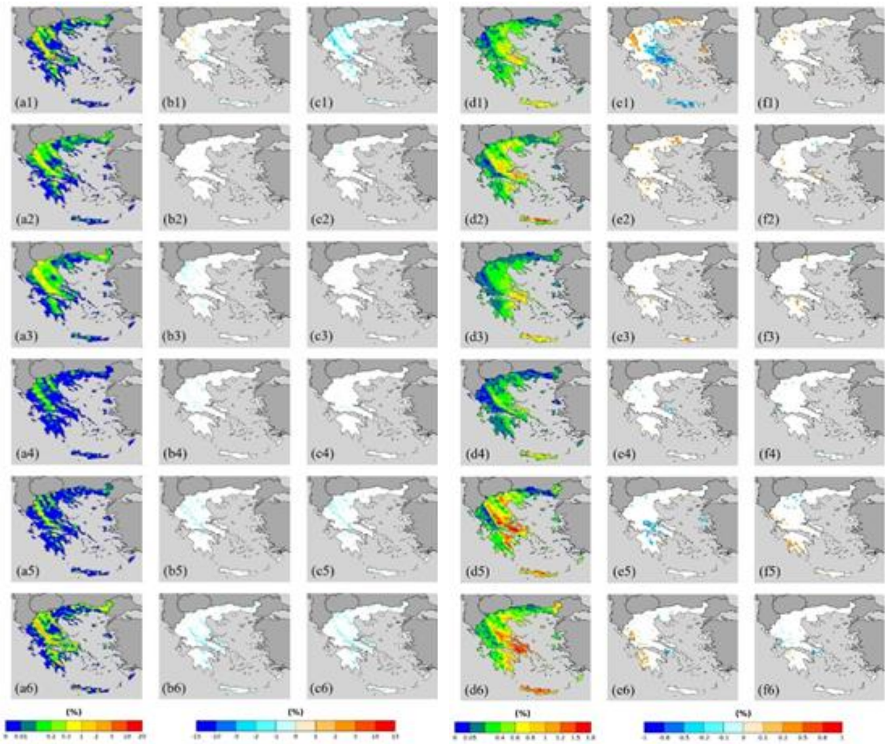

Figure 26: (a-c) RR20-ID and (d-f) RR95p-TX5p probabilities. Models 1: CNRM, 2: KNMI, 3: CLMcom, 4: SMHI, 5: DMI, 6: WRF_EC. (a, d) 1980-2004, (b, e) (2025-2049 RCP 4.5) – (1980-2004) and (c, f) (2025-2049 RCP 8.5) – (1980-2004).

Figure 26a shows that RR20-ID events are limited to mountainous areas. Again, CNRM exhibits in few areas the most extreme values ranged between 10% to 20%. Similar values are, also exhibited by WRF_EC. These models display the most extreme reduction of the probabilities in the future, reaching 10% to 15 % in the case of CNRM and RCP8.5. WRF_EC, DMI and to a lesser degree KNMI in Figure 26d, yield the most extreme probabilities for RR95p-TX5p events that reach 1%. The most notable changes are displayed by CNRM under RCP4.5, which shows increases in western and northern parts of the country and significant decreases in eastern areas and Crete.

Conclusions

This work presents for the first time to our knowledge an extensive study of wet-cold compound events in Greece for the historical and future periods of 1980-2004 and 2025-2049, respectively. Models' data from EUROCORDEX initiative of 0.11° resolution and reanalysis data (ERA5 and ERA-Interim dynamically downscaled to 5km^2) were used and validated for the determined WCCEs against the formally available observational datasets by HNMS for the country. The number of events and their probabilities of occurrence were determined by applying two different approaches, fixed thresholds and percentiles. Then, the validation of the models' datasets against observations was performed for the determined thresholds (univariate and bivariate) and the 20-years return levels using blog-maxima and POT methods. The probability of WCCEs was computed using the empirical method and the best-fitted copula for the bivariate timeseries. Moreover, for the reanalysis data, we applied the approach of the most common copula of the 21 observational stations.

Even though reanalysis and projection models seemed to underestimate extreme precipitation, thus leading to less extreme events, both helped to map the geographical distribution of WCCEs over Greece.

All models agreed that for the historical period, more events by the fixed threshold approach were found over mountainous regions while the percentile approach yielded more WCCEs over the eastern parts of the country and Crete.

Furthermore, the projected changes in the number of WCCEs were investigated under RCP 4.5 and RCP 8.5. Significant changes were obtained using the fixed threshold method over mountainous areas which showed a potential reduction of the number of compound events particularly under RCP 8.5. The application of the percentile method yielded reduced changes in the probabilities of wet-cold compounds than the fixed threshold approach while the models showcased higher disagreement among them concerning the changes.

The reduction of RR20-FD and RR20-ID WCCEs on mountains that most models predicted for the future, might mean less heavy snowfall events and possibly less accumulated snow depth. If such a scenario will be verified, Greece faces the threat of losing main sources of fresh water that come from melted mountain snow during spring or early summer. The change of WCCEs for RR95p-(TN5p or TX5p) does not necessarily translate to a corresponding change of snowfall events, since the temperature percentile thresholds are for several occasions higher than 0 °C. Snow events may occur at higher temperatures, however in this study we examined the amount of precipitation and not its type. Next future steps could focus on the investigation of the synoptic systems that cause wet-cold compound events in the area of interest. The higher resolution reanalysis and projection simulations used in the study, WRF_ERA_I and WRF_EC, exhibited with greater detail the distribution of WCCEs, highlighting the need for high resolution model data for areas with diverse topography like Greece.

Acknowledgments

The authors acknowledge partial funding by the project "National Research Network for Climate Change and its Impacts, (CLIMPACT - 105658/17-10-2019)" of the Ministry of Development, GSRT, Program of Public Investment, 2019.

References

Abdi, H.: The Kendall Rank Correlation Coefficient, 2007.

Abraj, M. A. M. and Hewaarachchi, A. P.: Joint return period estimation of daily maximum and minimum temperatures using copula method, 66, 175–190, https://doi.org/10.17654/AS066020175, 2021.

Aghakouchak, A., Chiang, F., Huning, L. S., Love, C. A., Mallakpour, I., Mazdiyasni, O., Moftakhari, H., Papalexiou, S. M., Ragno, E., and Sadegh, M.: Climate Extremes and Compound Hazards in a Warming World, 48, 519–548, https://doi.org/10.1146/ANNUREV-EARTH-071719-055228, 2020.

Akaike, H.: A New Look at the Statistical Model Identification, 19, 716–723, https://doi.org/10.1109/TAC.1974.1100705, 1974.

Anagnostopoulou, C. and Tolika, K.: Extreme precipitation in Europe: Statistical threshold selection based on climatological criteria, 107, 479–489, https://doi.org/10.1007/S00704-011-0487-8/TABLES/2, 2012.

Balkema, A. A. and Haan, L. de: Residual Life Time at Great Age, 2, 792–804, https://doi.org/10.1214/AOP/1176996548, 1974.

Bommier, E.: Peaks-Over-Threshold Modelling of Environmental Data, 2014.

Christensen, O. B.: Regional climate change in Denmark according to a global 2-degree-warming scenario, 2006.

Coles, S.: An Introduction to Statistical Modeling of Extreme Values, https://doi.org/10.1007/978-1-4471-3675-0, 2001.

https://doi.org/10.5194/egusphere-2022-48
Preprint. Discussion started: 27 April 2022

Cong, R. G. and Brady, M.: The interdependence between rainfall and temperature: Copula analyses, 2012, https://doi.org/10.1100/2012/405675, 2012.

Curtis, S., Fair, A., Wistow, J., Val, D. v., and Oven, K.: Impact of extreme weather events and climate change for health and social care systems, 16, 23–32, https://doi.org/10.1186/S12940-017-0324-3/METRICS, 2017.

Demiroglu, O. C., Kučerová, J., and Ozcelebi, O.: Snow reliability and climate elasticity: Case of a Slovak ski resort, 70, 1–12, https://doi.org/10.1108/TR-01-2014-0003/FULL/PDF, 2015.

Dzupire, N. C., Ngare, P., and Odongo, L.: A copula based bi-variate model for temperature and rainfall processes, 8, e00365, https://doi.org/10.1016/J.SCIAF.2020.E00365, 2020.

Fisher, R. A. and Tippett, L. H. C.: Limiting forms of the frequency distribution of the largest or smallest member of a sample, 24, 180–190, https://doi.org/10.1017/S0305004100015681, 1928.

Fonseca, D., Carvalho, M. J., Marta-Almeida, M., Melo-Gonçalves, P., and Rocha, A.: Recent trends of extreme temperature indices for the Iberian Peninsula, 94, 66–76, https://doi.org/10.1016/J.PCE.2015.12.005, 2016.

García-Ruiz, J. M., López-Moreno, I. I., Vicente-Serrano, S. M., Lasanta-Martínez, T., and Beguería, S.: Mediterranean water resources in a global change scenario, 105, 121–139, https://doi.org/10.1016/J.EARSCIREV.2011.01.006, 2011.

Gilleland, E. and Katz, R. W.: extRemes 2.0: An Extreme Value Analysis Package in R, 72, 1–39, https://doi.org/10.18637/JSS.V072.I08, 2016.

Gnedenko, B.: Sur La Distribution Limite Du Terme Maximum D'Une Serie Aleatoire, 44, 423, https://doi.org/10.2307/1968974, 1943.

Goda, Y.: Inherent Negative Bias of Quantile Estimates of Annual Maximum Data Due to Sample Size Effect: A Numerical Simulation Study, 53, 397–429, https://doi.org/10.1142/S0578563411002409, 2018.

Goulden, C.: Methods of statistical analysis., 1939.

Hao, Z., Singh, V. P., and Hao, F.: Compound Extremes in Hydroclimatology: A Review, 10, 718, https://doi.org/10.3390/W10060718, 2018.

Hersbach, H., Bell, B., Berrisford, P., Hirahara, S., Horányi, A., Muñoz-Sabater, J., Nicolas, J., Peubey, C., Radu, R., Schepers, D., Simmons, A., Soci, C., Abdalla, S., Abellan, X., Balsamo, G., Bechtold, P., Biavati, G., Bidlot, J., Bonavita, M., de Chiara, G., Dahlgren, P., Dee, D., Diamantakis, M., Dragani, R., Flemming, J., Forbes, R., Fuentes, M., Geer, A., Haimberger, L., Healy, S., Hogan, R. J., Hólm, E., Janisková, M., Keeley, S., Laloyaux, P., Lopez, P., Lupu, C., Radnoti, G., de Rosnay, P., Rozum, I., Vamborg, F., Villaume, S., and Thépaut, J. N.: The ERA5 global reanalysis, 146, 1999–2049, https://doi.org/10.1002/QJ.3803, 2020.

Hochman, A., Marra, F., Messori, G., Pinto, J., Raveh-Rubin, S., Yosef, Y., and Zittis, G.: ESD Reviews: Extreme Weather and Societal Impacts in the Eastern Mediterranean, 1–53, https://doi.org/10.5194/ESD-2021-55, 2021.

Houston, T. G., Changnon, S. A., Ae, T. G. H., and Changnon, S. A.: Freezing rain events: a major weather hazard in the conterminous US, 40, 485–494, https://doi.org/10.1007/S11069-006-9006-0, 2006.

James Pickands: Statistical Inference Using Extreme Order Statistics, 3, 119–131, https://doi.org/10.1214/AOS/1176343003, 1975.

Konisky, D. M., Hughes, L., and Kaylor, C. H.: Extreme weather events and climate change concern, 134, 533–547, https://doi.org/10.1007/S10584-015-1555-3/FIGURES/3, 2016.

Kundzewicz, Z. W., Radziejewski, M., and Pińskwar, I.: Precipitation extremes in the changing climate of Europe, 31, 51–58, https://doi.org/10.3354/CR031051, 2006.

https://doi.org/10.5194/egusphere-2022-48
Preprint. Discussion started: 27 April 2022

Lazoglou, G. and Anagnostopoulou, C.: Joint distribution of temperature and precipitation in the Mediterranean, using the Copula method, 135, 1399–1411, https://doi.org/10.1007/S00704-018-2447-Z/FIGURES/5, 2019.

Leonard, M., Westra, S., Phatak, A., Lambert, M., van den Hurk, B., Mcinnes, K., Risbey, J., Schuster, S., Jakob, D., and Stafford-Smith, M.: A compound event framework for understanding extreme impacts, 5, 113–128, https://doi.org/10.1002/WCC.252, 2014.

Llasat, M. C., Turco, M., Quintana-Seguí, P., and Llasat-Botija, M.: The snow storm of 8 March 2010 in Catalonia (Spain): a paradigmatic wet-snow event with a high societal impact, 14, 427–441, https://doi.org/10.5194/NHESS-14-427-2014, 2014.

de Luca, P., Messori, G., Faranda, D., Ward, P. J., and Coumou, D.: Compound warm-dry and cold-wet events over the Mediterranean, 11, 793–805, https://doi.org/10.5194/ESD-11-793-2020, 2020.

Markantonis, I., Vlachogiannis, D., Sfetsos, T., Kioutsioukis, I., and Politi, N.: An Investigation of cold-wet Compound Events in Greece, https://doi.org/10.5194/EMS2021-188, 2021.

van Meijgaard, E., van Ulft, L. H., van de Berg, W. J., Bosveld, F. C., van den Hurk, B. J. J. M., Lenderink, G., and Siebesma, A. P.: The KNMI regional atmospheric climate model RACMO version 2.1, 2008.

Moalafhi, D. B., Evans, J. P., and Sharma, A.: Evaluating global reanalysis datasets for provision of boundary conditions in regional climate modelling, 47, 2727–2745, https://doi.org/10.1007/S00382-016-2994-X/TABLES/9, 2016.

Moberg, A., Jones, P. D., Lister, D., Walther, A., Brunet, M., Jacobeit, J., Alexander, L. v., Della-Marta, P. M., Luterbacher, J., Yiou, P., Chen, D., Tank, A. M. G. K., Saladié, O., Sigró, J., Aguilar, E., Alexandersson, H., Almarza, C., Auer, I., Barriendos, M., Begert, M., Bergström, H., Böhm, R., Butler, C. J., Caesar, J., Drebs, A., Founda, D., Gerstengarbe, F. W., Micela, G., Maugeri, M., Österle, H., Pandzic, K., Petrakis, M., Srnec, L., Tolasz, R., Tuomenvirta, H., Werner, P. C., Linderholm, H., Philipp, A., Wanner, H., and Xoplaki, E.: Indices for daily temperature and precipitation extremes in Europe analyzed for the period 1901–2000, 111, 22106, https://doi.org/10.1029/2006JD007103, 2006.

Nelsen, R.: An introduction to copulas, 2007.

Pandey, P. K., Das, L., Jhajharia, D., and Pandey, V.: Modelling of interdependence between rainfall and temperature using copula, 4, 867–879, https://doi.org/10.1007/S40808-018-0454-9, 2018.

Pestereva, N. M., Popova, N. Yu., and Shagarov, L. M.: Modern Climate Change and Mountain Skiing Tourism: the Alps and the Caucasus, 1602–1617, 2012.

Politi, N., Nastos, P. T., Sfetsos, A., Vlachogiannis, D., and Dalezios, N. R.: Evaluation of the AWR-WRF model configuration at high resolution over the domain of Greece, 208, 229–245, https://doi.org/10.1016/J.ATMOSRES.2017.10.019, 2018.

Politi, N., Sfetsos, A., Vlachogiannis, D., Nastos, P. T., and Karozis, S.: A Sensitivity Study of High-Resolution Climate Simulations for Greece, 8, 44, https://doi.org/10.3390/CLI8030044, 2020.

Politi, N., Vlachogiannis, D., Sfetsos, A., and Nastos, P. T.: High-resolution dynamical downscaling of ERA-Interim temperature and precipitation using WRF model for Greece, 57, 799–825, https://doi.org/10.1007/S00382-021-05741-9/FIGURES/17, 2021.

Politi, N., Vlachogiannis, D., Sfetsos, A., Nastos, P.T., High resolution projections for extreme temperatures and precipitation over Greece, under review, https://doi.org/10.21203/rs.3.rs-1263740/v1, 2022

Pongrácz, R., Bartholy, J., Gelybó, G., and Szabó, P.: Detected and expected trends of extreme climate indices for the carpathian basin, 15–28, https://doi.org/10.1007/978-1-4020-8876-6_2, 2009.

https://doi.org/10.5194/egusphere-2022-48
Preprint. Discussion started: 27 April 2022

Poschlod, B.: Using high-resolution regional climate models to estimate return levels of daily extreme precipitation over Bavaria, 21, 3573–3598, https://doi.org/10.5194/NHESS-21-3573-2021, 2021.

Raziei, T., Daryabari, J., Bordi, I., Modarres, R., and Pereira, L. S.: Spatial patterns and temporal trends of daily precipitation indices in Iran, 124, 239–253, https://doi.org/10.1007/S10584-014-1096-1/TABLES/1, 2014.

Rockel, B., Will, A., and Hense, A.: The regional climate model COSMO-CLM (CCLM), 17, 347–348, https://doi.org/10.1127/0941-2948/2008/0309, 2008.

Sadegh, M., Moftakhari, H., Gupta, H. v., Ragno, E., Mazdiyasni, O., Sanders, B., Matthew, R., and AghaKouchak, A.: Multihazard Scenarios for Analysis of Compound Extreme Events, 45, 5470–5480, https://doi.org/10.1029/2018GL077317, 2018.

Samuelsson, P., Jones, C. G., Willén, U., Ullerstig, A., Gollvik, S., Hansson, U., Jansson, C., Kjellström, E., Nikulin, G., and Wyser, K.: The Rossby Centre Regional Climate model RCA3: model description and performance, 63, 4–23, https://doi.org/10.1111/J.1600-0870.2010.00478.X, 2016.

Schepsmeier, U., Stoeber, J., Christian, E., and Maintainer, B.: Package "VineCopula" Type Package Title Statistical inference of vine copulas, 2013.

Singh, H., Najafi, M. R., and Cannon, A. J.: Characterizing non-stationary compound extreme events in a changing climate based on large-ensemble climate simulations, 56, 1389–1405, https://doi.org/10.1007/S00382-020-05538-2/FIGURES/6, 2021.

Sklar and M.: Fonctions de repartition a n dimensions et leurs marges, 8, 229–231, 1959.

Spiridonov, V., Somot, S., and Déqué, M.: ALADIN-Climate: from the origins to present date, n.d.

Tavakol, A., Rahmani, V., and Harrington, J.: Probability of compound climate extremes in a changing climate: A copula-based study of hot, dry, and windy events in the central United States, 15, 104058, https://doi.org/10.1088/1748-9326/ABB1EF, 2020.

Tošić, I. and Unkašević, M.: Extreme daily precipitation in Belgrade and their links with the prevailing directions of the air trajectories, 111, 97–107, https://doi.org/10.1007/S00704-012-0647-5/FIGURES/9, 2013.

Trujillo, E., Molotch, N. P., Goulden, M. L., Kelly, A. E., and Bales, R. C.: Elevation-dependent influence of snow accumulation on forest greening, 5, 705–709, https://doi.org/10.1038/ngeo1571, 2012.

Vajda, A., Tuomenvirta, H., Juga, I., Nurmi, P., Jokinen, P., and Rauhala, J.: Severe weather affecting European transport systems: The identification, classification and frequencies of events, 72, 169–188, https://doi.org/10.1007/S11069-013-0895-4/TABLES/3, 2014.

Vogel, J., Paton, E., and Aich, V.: Seasonal ecosystem vulnerability to climatic anomalies in the Mediterranean, 18, 5903–5927, https://doi.org/10.5194/BG-18-5903-2021, 2021.

Zanocco, C., Boudet, H., Nilson, R., Satein, H., Whitley, H., and Flora, J.: Place, proximity, and perceived harm: extreme weather events and views about climate change, 149, 349–365, https://doi.org/10.1007/S10584-018-2251-X/TABLES/2, 2018.

Zhang, W., Luo, M., Gao, S., Chen, W., Hari, V., and Khouakhi, A.: Compound Hydrometeorological Extremes: Drivers, Mechanisms and Methods, 9, 941, https://doi.org/10.3389/FEART.2021.673495/BIBTEX, 2021.

Zscheischler, J. and Seneviratne, S. I.: Dependence of drivers affects risks associated with compound events, 3, https://doi.org/10.1126/SCIADV.1700263/SUPPL_FILE/1700263_SM.PDF, 2017.

Zscheischler, J., Orth, R., and Seneviratne, S. I.: Bivariate return periods of temperature and precipitation explain a large fraction of European crop yields, 14, 3309–3320, https://doi.org/10.5194/BG-14-3309-2017, 2017.

https://doi.org/10.5194/egusphere-2022-48
Preprint. Discussion started: 27 April 2022

Zscheischler, J., Westra, S., van den Hurk, B. J. J. M., Seneviratne, S. I., Ward, P. J., Pitman, A., AghaKouchak, A., Bresch, D. N., Leonard, M., Wahl, T., and Zhang, X.: Future climate risk from compound events, 8, 469–477, https://doi.org/10.1038/s41558-018-0156-3, 2018.

Code and data availability

Code and results data available upon request.

Author contributions

IM has worked on conceptualization, methodology, validation, visualization, investigation, writing review and editing. AS, DV and IK contributed on conceptualization, review and supervision. All authors have read and agreed to the published version of the manuscript.

Competing interests

The authors declare that they have no conflict of interest.

Appendix A

NUMBER	LOCATION	ID	LATITUDE	LONGITUDE	ELEVATION (m)
1	Alexandroupoli	16627	40.85	25.917	4
2	Elliniko	16716	37.8877	23.7333	10
3	Ioannina	16642	39.7	20.817	483
4	Irakleio	16754	35.339	25.174	39
5	Kalamata	16726	37.067	22.017	6
6	Kastoria	16614	40.45	21.28	660.95
7	Kerkira	16641	39.603	19.912	1
8	Kithira	16743	36.2833	23.0167	167
9	Larisa	16648	39.65	22.417	73
10	Limnos	16650	39.9167	25.2333	4
11	Methoni	16734	36.8333	21.7	34
12	Milos	16738	36.7167	24.45	183
13	Mitilini	16667	39.059	26.596	4
14	Naxos	16732	37.1	25.383	9
15	Rhodes	16749	36.42896	28.21661	95
16	Samos	16723	37.79368	26.68199	10
17	Skyros	16684	38.9676	24.4872	12
18	Souda	16746	35.4833	24.1167	151
19	Thessaloniki	16622	40.517	22.967	2
20	Tripoli	16710	37.527	22.401	651
21	Zakinthos	16719	37.751	20.887	5

Table A1: HNMS stations information.

https://doi.org/10.5194/egusphere-2022-48
Preprint. Discussion started: 27 April 2022

Appendix B

	HNMS	CNRM	KNMI	CLMcom	SMHI	DMI	WRF_EC	ERA5	WRF_ERA_I
Alexandroupoli	Rot. BB8 270	Rot Tawn type 2 270	Rot Tawn type 2 270	Survival BB8	Rot BB8 90 deg	Rot Tawn type 1 180	Gaussian	Frank	Rot BB8 270
Elliniko	Frank	Rot. BB8 270	Rot BB8 90	Rot Tawn type 1 180	Rot Tawn type 2 90	Rot Tawn type 1 180	Clayton	Rot Gumbel 270	Clayton
Ioannina	Rot. BB8 270	Rot BB8 90	Rot BB8 90	Rot Tawn type 1 270	Rot BB8 270	Rot Tawn type 2 90	Rot Tawn type 1 270	Rot BB8 270	Rot Tawn type 1 270
Irakleio	Gaussian	Rot BB8 270	Rot Joe 270	Frank	Rot Tawn type 1 270	Clayton	Gaussian	BB8	Survival BB8
Kalamata	Gaussian	Rot Tawn type 1 270	Frank	Survival BB8	Rot Tawn type 2 90	Clayton	Rot Tawn type 1 270	Rot BB8 270	Rot Tawn type 2 180
Kastoria	Rot BB8 270	Rot BB8 90 deg	Rot BB8 90	Survival Joe	T	RotTawn type 1 180	Rot Tawn type 1 270	Rot BB8 270	Rot Tawn type 1 270
Kerkira	Rot BB8 270	Rot Tawn type 2 270	Rot BB8 270	Survival BB8	Rot BB8 270	Rot Tawn type 2 90	Rot Clayton 90	Gaussian	Rot Clayton 90
Kithira	Survival BB8	Tawn type 1	Gaussian	Survival BB8	Gaussian	Rot Tawn type 1 180	Gaussian	Frank	Rot Tawn type 2 180
Larisa	Rot BB8 270	T	Frank	Survival BB8	T	Rot Tawn type 1 180	Rot BB8 270	Rot BB8 270	RotTawn type 1 270
Limnos	Rot BB8 270	Rot Tawn type 2 270	Frank	Survival BB8	Gaussian	Rot Tawn type 1 180	Tawn type 1	BB8	Rot Clayton 90
Methoni	Rot Tawn type 2 180	Rot BB8 270	Rot BB8 270	Clayton	Gaussian	Rot Tawn type 1 180	Rot Tawn type 1 270	Rot Tawn type 1 270	Clayton
Milos	Gaussian	BB8	Gaussian	Survival BB8	Gaussian	Rot Tawn type 1 180	BB8	BB8	Gaussian
Mitilini	Rot BB8 270	Rot BB8 270	Frank	Rot Tawn type 1 180	Rot BB8 90	Rot Tawn type 1 180	Rot Tawn type 1 270	Frank	Rot BB8 270
Naxos	Survival BB8	BB8	Rot Tawn type 2 270	Survival BB8	Rot Tawn type 1 270	Rot Tawn type 1 180	Gaussian	BB8	Rot Tawn type 2 180
Rhodes	Rot Tawn type 2 180	Tawn type 1	Rot Tawn type 2 180	Survival BB8	Gaussian	Rot Tawn type 1 180	Rot Tawn type 1 270	Rot Tawn type 2 180	Rot Tawn type 1 270
Samos	Rot BB8 270	Rot Clayton 90	Rot BB8 90	Rot Tawn type 1 180	Rot BB8 90	Rot Tawn type 1 180	Rot BB8 270	Rot BB8 270	Rot Clayton 90
Skyros	Rot Tawn type 2 180	BB8	Rot Tawn type 2 270	Survival BB8	Rot Tawn type 2 90	Rot Tawn type 1 180	BB8	BB8	Gaussian
Souda	Gaussian	Clayton	Tawn type 1	Survival BB8	Rot Tawn type 1 270	BB7	Gaussian	BB8	Survival BB8
Thessaloniki	Rot BB8 270	Rot Tawn type 1 270	Frank	Survival BB8	Rot BB8 90 d	Rot Tawn type 1 180	Rot Clayton 90	Rot Joe 270	Rot Tawn type 1 270
Tripoli	Rot BB8 270	Rot Tawn type 1 270	Rot BB8 90	Survival BB8	Rot Tawn type 1 270	Clayton	Rot Tawn type 2 180	Rot BB8 270	Clayton
Zakinthos	Rot Tawn type 2 90	Rot BB8 270	Rot BB8 270	Survival BB8	T	Rota Tawn type 1 180	Rot Tawn type 1 270	Frank	Rot Tawn type 1 270

Table B1: (-TN, RR) best-fitted Copula for each station timeseries.

	HNMS	CNRM	KNMI	CLMcom	SMHI	DMI	WRF_EC	ERA5	WRF_ERA_I
Alexandroupoli	Rot Tawn type 1 270	Rot BB8 270	Frank	Rot Tawn type 1 180	Rot Tawn type 1 270	Rot Tawn type 2 90	Rot Tawn type 2 180	Independence	Rota Tawn type 2 180
Elliniko	Survival BB8	Rot BB8 270	Rot Clayton 270	Rot Tawn type 1 180	Clayton	Rot Tawn type 1 180	Gaussian	Gaussian	Gaussian
Ioannina	Rot Tawn type 2 180	Rot Tawn type 2 180	Rot Tawn type 2 180	Survival BB8	Rot Tawn type 2 180	Survival BB8	Rot Tawn type 2 180	Frank	Rot Tawn type 2 180
Irakleio	BB8	Gaussian	Survival BB1	Frank	T	Gaussian	Gaussian	BB8	Frank
Kalamata	Survival BB8	Rot Tawn type 2 180	Rot Tawn type 2 180	Survival BB8	Survival BB8	Survival BB8	Rot Tawn type 2 180	Rot Tawn type 2 180	Rot Tawn type 2 180
Kastoria	Survival BB8	Rot Tawn type 2 180	Rot Tawn type 2 180	Survival BB8	Rot Tawn type 2 180	Survival BB8	Rot Tawn type 2 180	Gaussian	Rot Tawn type 2 180
Kerkira	Survival BB8	T	Gaussian	Survival BB8	Rot Tawn type 2 180	Rot Tawn type 2 90	Rot Tawn type 1 270	Rot Tawn type 2 180	Rot Tawn type 2 180
Kithira	Survival BB8	Tawn type 1	Clayton	Survival BB8	Survival BB8	Survival BB8	Gaussian	Rot Tawn type 1 180	Rot Tawn type 2 180
Larisa	Survival BB8	Survival BB8	Tawn type 1	Survival BB8	Rot Tawn type 2 180	Survival BB8	Rot Tawn type 2 180	BB8	Rot Tawn type 2 180
Limnos	Rot Tawn type 2 180	Rot Tawn type 2 180	Rot Tawn type 2 180	Survival BB8	Rot Tawn type 1 270	Survival BB8	Gaussian	Tawn type 2	Tawn type 1
Methoni	Frank	T	Rot Tawn type 2 180	Survival BB8	Survival BB8	Survival BB8	Rot Tawn type 1 270	Survival BB8	Survival BB8
Milos	Survival BB8	Rot Tawn type 2 180	Rot Tawn type 1 180	Survival BB8	Survival BB8	Survival BB8	Gaussian	BB8	Frank
Mitilini	Rot Tawn type 2 180	Rot BB8 270	Rot BB8 270	Survival BB8	Rot Tawn type 2 180	Rot Tawn type 1 180	Rot Tawn type 2 180	Rot BB8 270	Rot Tawn type 2 180
Naxos	Survival BB8	Rot Tawn type 2 270	Rot Tawn type 1 180	Survival BB8	Survival BB8	Survival BB8	Gaussian	Tawn type 2	Rot Tawn type 2 180
Rhodes	Survival BB8	Tawn type 1	Rot Tawn type 1 270	Survival BB8	Survival BB8	Rot Tawn type 1 180	Rot Tawn type 2 180	Rot Tawn type 2 180	Rot Tawn type 2 180
Samos	Rot Tawn type 2 180	Rot Clayton 90	Rot BB8 270	Rot Tawn type 2 180	Rot Tawn type 2 180	Survival BB8	Rot Tawn type 2 180	Rot BB8 270	Rot Tawn type 2 180
Skyros	Gaussian	Rot Tawn type 2 180	Tawn type 2	Survival BB8	Survival BB8	Survival BB8	Gaussian	BB8	Survival BB8
Souda	Frank	Gaussian	Gaussian	Frank	T	Gaussian	Gaussian	Frank	BB8
Thessaloniki	Gaussian	T	Tawn type 1	Survival BB8	Rot Tawn type 2 180	Survival BB8	Tawn type 1	Rot Tawn type 2 180	Rot Tawn type 2 180
Tripoli	Survival BB8	Rot Tawn type 2 180	Survival BB8	Survival BB8	Survival BB8	Survival BB8	Survival BB8	Survival BB8	Survival BB8
Zakinthos	Frank	Rot Tawn type 2 180	Rot Tawn type 2 180	Survival BB8	Survival BB8	Survival BB8	Rot Tawn type 2 180	Frank	Rot Tawn type 2 180

Table B2: (-TX, RR) best-fitted Copula for each station timeseries.